Title

Presence of Delocalized Ti 3d Electrons in Ultrathin Single-Crystal SrTiO3

Journal

Nano Letters, 22(4)

ISSN

1530-6984

Authors

Chiu, Chun-Chien

Ho, Sheng-Zhu

Lee, Jenn-Min

et al.

Publication Date

2022-02-23

DOI

10.1021/acs.nanolett.1c04434

Presence of delocalized Ti 3*d* electrons in ultra-thin single crystal $SrTiO_3$

Chun-Chien Chiu,[†,Δ] *Sheng-Zhu Ho,*[†,Δ] *Jenn-Min Lee,*[‡] *Yu-Cheng Shao,*[§,∥] *Yang Shen,*[⊥] *Yu-Chen Liu,*[†] *Yao-Wen Chang,*[†] *Yun-Zhe Zheng,*[⊥] *Rong Huang,*[⊥] *Chun-Fu Chang,*[#] *Chang-Yang Kuo,*[&] *Chun-Gang Duan,*[⊥] *Shih-Wen Huang,*[▽,‡,*] *Jan-Chi Yang,*[†,$,*] *and Yi-De Chuang*[§,*]

[†] Department of Physics, National Cheng Kung University, Tainan 701, Taiwan

[‡] MAX IV Laboratory, Lund University, P. O. Box 118, 221 00 Lund, Sweden

[§] Advanced Light Source, Lawrence Berkeley National Laboratory, Berkeley, CA 94720, USA

[⊥] Key Laboratory of Polar Materials and Devices, Ministry of Education, Department of Electronics, East China Normal University, Shanghai 200241, China

[#] Max-Planck Institute for Chemical Physics of Solids, Dresden, 01187, Germany

[&] Department of Electrophysics, National Chiao Tung University, Hsinchu 30010, Taiwan

[▽] Swiss Light Source, Paul Scherrer Institut, CH5232 Villigen PSI, Switzerland

[$] Center for Quantum Frontiers of Research & Technology (QFort), National Cheng Kung University, Tainan 70101, Taiwan

[Δ] These authors contributed equally in this work

KEYWORDS

freestanding $SrTiO_3$, ferroelectricity, delocalized Ti 3*d* electrons, RIXS

ABSTRACT

Strontium titanate (STO), with a wide spectrum of emergent properties such as ferroelectricity and superconductivity, has received significant attention in the community of strongly correlated materials. In the strain-free STO film grown on $SrRuO_3$ buffer layer, the existing polar nanoregions can facilitate the room temperature ferroelectricity when STO film thickness approaches 10 nm. Here, we show that around this thickness scale, the freestanding STO films without the influence of substrate show the tetragonal structure at room temperature, contrasting to the cubic structure seen in bulk form. The spectroscopic measurements reveal the modified Ti-O orbital hybridization that causes the Ti ion to deviate from its nominal 4+ valency ($3d^0$ configuration) with excess delocalized 3*d* electrons. Additionally, the Ti ion in TiO_6 octahedron exhibits an off-center displacement. The inherent symmetry-lowering in ultra-thin freestanding films offers an alternative way to achieve tunable electronic structures that are of paramount importance for future technological applications.

TEXT

Bulk strontium titanate ($SrTiO_3$, STO) is a quantum paraelectric insulator that exhibits an antiferrodistortive structural transition from high temperature cubic phase (Pm3m) to low temperature tetragonal phase (P4mm) around 105 K. Accompanying this structural transition is the softening of zone-center transverse optical (TO) phonon responsible for the ferroelectricity (FE) in other titanates like $PbTiO_3$ and $BaTiO_3$. But unlike these titanates, the quantum zero-point motion in STO prohibits the Ti ion from staying at an off-center position in TiO_6 octahedron, causing the dielectric constant to deviate from the Curie-Weiss law below 36 K and suppressing the ferroelectricity down to the lowest temperature.[1,2] With decades of research on its properties and perfection in its growth, STO has become one of the most widely used materials in oxide thin films and heterostructures.[3,4] These thin films and heterostructures have attracted great attention because of the emergent properties found at the interfaces.[5,6] Examples such as the electric-field tunable two-dimensional electron gas (2DEG), magnetism, and superconductivity at the interface of insulating $LaAlO_3$ and TiO_2-terminated $SrTiO_3$,[7-11] the interfacial charge modulation in $LaTiO_3/SrTiO_3$ heterostructure,[12,13] the enhanced superconductivity in monolayer pnictide grown on STO ($FeSe/SrTiO_3$),[14,15] to name a few, demonstrate the rich structural and electronic reconstructions.[16,17]

The strong tendency for inducing these properties in STO-based thin films and heterostructures is partly related to the structural instability of STO itself. Even for STO film alone, it has been shown that using external strain, electric field, oxygen vacancies, and oxygen isotope can suppress quantum frustration and stabilize the incipient ferroelectricity.[18-23] Applying strain also enhances the dilute superconductivity in STO.[24,25] Moreover, depending on the growth condition that varies the concentration of oxygen vacancies, there are reports of bulk and/or surface conducting

carries.[26-28] These studies are all performed on STO bulk and thin films grown on strained or unstrained substrates (using a $SrRuO_3$ buffer layer in between the STO and growth substrate) that are subjected to extrinsic modifications. There is a report of room temperature ferroelectricity facilitated by the polar nanoregions (PNR, presumably from the antisite Ti due to the Sr deficiency) in the so-called unstrained STO film when the film thickness approaches 10 nm;[21] however, the influence of buffer $SrRuO_3$ layer through the bridging oxygens, this unique length scale, and the nature of this Sr deficiency are overlooked. Here, we report that by simply reducing the thickness of pristine, insulating STO in the form of freestanding films (without the growth substrate) below 20 nm, the STO will attain the tetragonal structure at room temperature with bulk-like Ti 3*d* carries. This thickness scale is comparable to that of the PNR.[21]

The freestanding STO films (STO-FS) with thickness varying from 80 nm down to 5 nm were fabricated using the pulsed laser deposition (PLD) technique. The fabrication process is illustrated in Figure 1(a) and the details are listed in Supplementary Information (SI). Atomic force microscope (AFM) images of a 20 nm thick STO-FS taken before (Figure 1(b)) and after (Figure 1(c)) the freestanding treatment show the negligible change in topography and root-mean-square roughness (0.257 nm before and 0.299 nm after the treatment), affirming the preservation of film surface quality. We used x-ray diffraction (XRD) to determine the film thickness and room temperature in-plane (*a*-axis) and out-of-plane (*c*-axis) lattice constants. Figure 1(d) shows the XRD θ-2θ scan along the pseudo-cubic $(00L)_c$ direction. As film thickness decreases, the $(002)_c$ Bragg peak and Kiessig fringes broaden progressively. There is a visible shift in the $(002)_c$ Bragg peak position when the film thickness is 5 nm (red curve), which corresponds to an elongated *c*-axis. In the meantime, the azimuthal scan about $(013)_c$ peak shows a four-fold symmetry with a contracted *a*-axis (see Figure S1 in SI). Thickness-dependent lattice constants summarized in

Figure 1(e) reveal that, unlike bulk STO, the STO-FS loses its cubic structure at room temperature and becomes tetragonal when its thickness is 5 nm. Limited by the available data, we can only infer that the onset of room temperature tetragonality is in between 5 nm and 20 nm. Lowering the crystal symmetry from O_h to D_{4h} alters the electronic structure of Ti ion in TiO_6 octahedron, which can be further examined by x-ray spectroscopies.

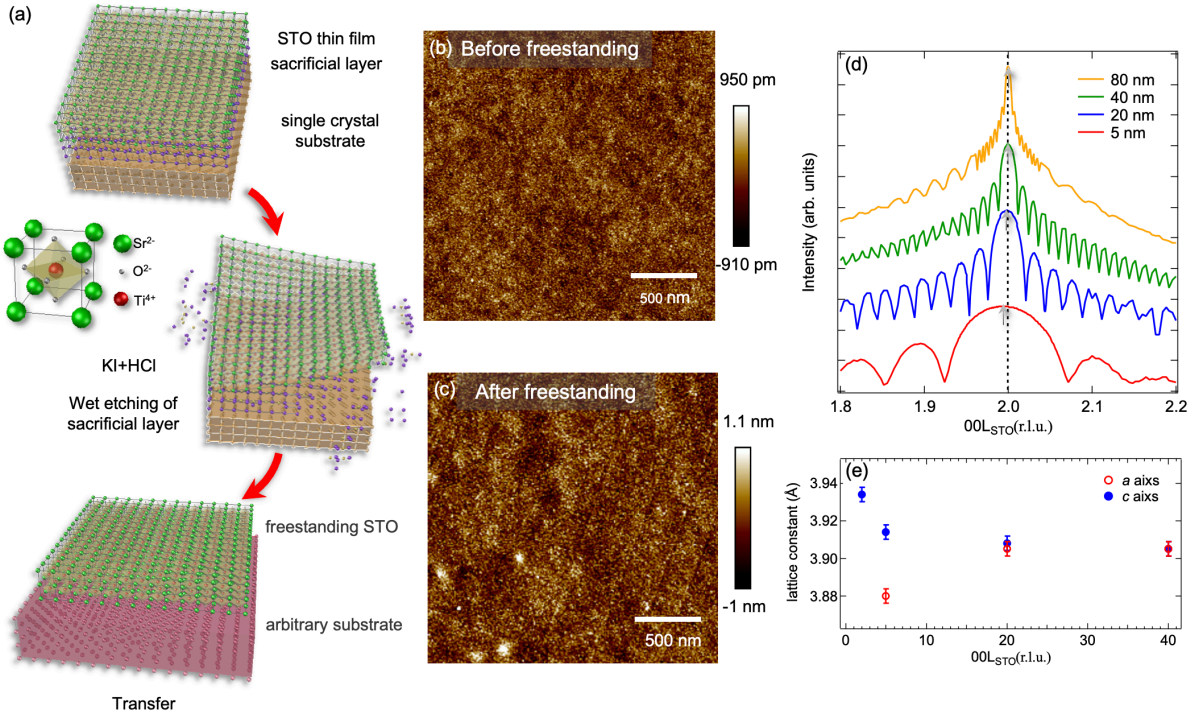

Figure 1. (a) Schematic illustration of the fabrication of freestanding STO thin films. (b, c) Atomic force microscope images of a 20 nm thick STO film on Si wafer support (b) before and (c) after the freestanding treatment. (d) XRD θ–2θ scan along the $(00L)_c$ direction showing the broadening and shift of $(002)_c$ Bragg peak in the 5 nm STO-FS. (e) *a*-axis (open red circles) and *c*-axis (filled blue circles) lattice constants obtained from XRD as a function of film thickness.

Figure 2(a) shows the Ti $L_{2,3}$-edge x-ray absorption (XAS) spectra recorded at room temperature from STO-FS and bulk STO (bare STO substrate, labeled STO). The bulk spectrum displays

spectral features that have been reported earlier.[29,30] This spectral lineshape can be explained by the atomic multiplet calculations using a $3d^0$ (Ti^{4+}) configuration in O_h symmetry. When STO-FS thickness is reduced, these spectral features remain mostly unchanged. However, at 5 nm thickness, a reduced crystal field energy 10Dq by 0.19 eV causes the e_g manifold to shift relative to the t_{2g} manifold. The broadening of e_g spectral lineshape at L_3 edge also suggests a slightly lower symmetry than O_h, consistent with the lattice constants in Figure 1(e).[30]

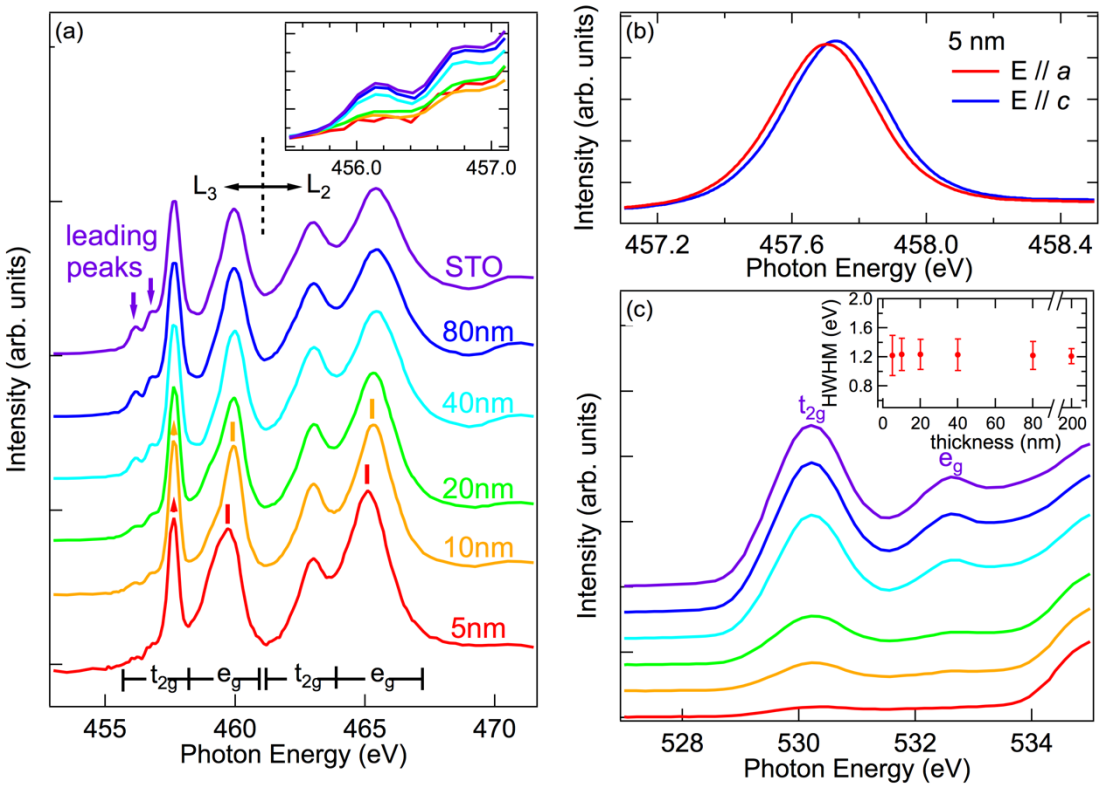

Figure 2. (a) Ti $L_{2,3}$-edge XAS spectra of bare STO substrate (labeled STO) and freestanding STO (STO-FS) films measured in total fluorescence yield (TFY) mode at room temperature. The inset shows the spectral profiles of the leading peaks marked by arrows. The movement of e_g manifold relative to the t_{2g} manifold is indicated by vertical bars. (b) X-ray linear dichroism (XLD) of a 5 nm STO-FS measured in total electron yield (TEY) mode. (c) O K-edge XAS spectra measured in TFY mode. The color schemes used in panels (a) and (c) are the same. The inset shows the half-

width at half-maximum (HWHM) of t_{2g} hybridization feature around 530 eV. The HWHM is measured on the lower energy side of the t_{2g} feature.

The lower crystal symmetry can manifest a dichroic effect in XAS spectra (x-ray linear dichroism, XLD) when one projects photon polarization along the in-plane (*a*-axis) and out-of-plane (*c*-axis) directions to probe the respective unoccupied Ti 3*d* orbitals.[31] By switching photon polarization from *c*-axis (blue curve) to *a*-axis (red curve), the energy of t_{2g} peak at L_3 edge (inverted triangle, Figure 2(a)) shifts by 28 meV relative to the e_g manifold that does not show this effect within our detection limit (see Figure 2(b)). This dichroic effect points to the lower energy for unoccupied *xy* orbital relative to the *xz*/*yz* orbitals. This effect can be explained by the configuration interaction cluster calculations with a substantial Ti ion displacement along the *c*-axis within D_{4h} symmetry (see Figure S4 in SI for more details). Offsetting the central Ti ion in TiO_6 octahedron breaks the inversion symmetry, a key ingredient for the ferroelectricity in titanates.[2,32-34] However, we will see in the later discussion that other factors in the ultra-thin STO-FS films prohibit the establishment of macroscopic ferroelectricity.

Besides the crystal symmetry and energies of spectral features, the Ti unoccupied density of states (DOS) also responds to the reduced film thickness. The inset in Figure 2(a) shows a monotonic decrease in the spectral weight of two leading peaks (arrows, Figure 2(a)). This spectral weight transfer into the occupied states implies that Ti ion deviates from its nominal 4+ valency ($3d^0$ configuration); or equivalently, there are additional 3*d* electrons in Ti in STO-FS. Comparing with the pure Ti^{3+} XAS spectra, we can exclude the possibility that these additional 3*d* electrons originate from oxygen vacancies in our samples (see Figure S5 in SI and later discussions). One finds a similar phenomenon for the high-mobility 2DEG at the interface of $LaAlO_3/SrTiO_3$

(LAO/STO). On the surface of STO films, whether induced by UV irradiation or high oxygen vacancy concentration, these Ti electrons will produce bands with different dimensionalities and effective masses.[26,27,35] Resonant inelastic x-ray scattering spectroscopy (RIXS) has been used to differentiate the delocalized and localized nature of these carriers in LAO/STO.[36-40] In Figure 3(a) and Figure 3(b), we show the incident photon energy dependent RIXS spectra (RIXS map) from 20 nm and 75 nm STO-FS, respectively, to offer a global view.

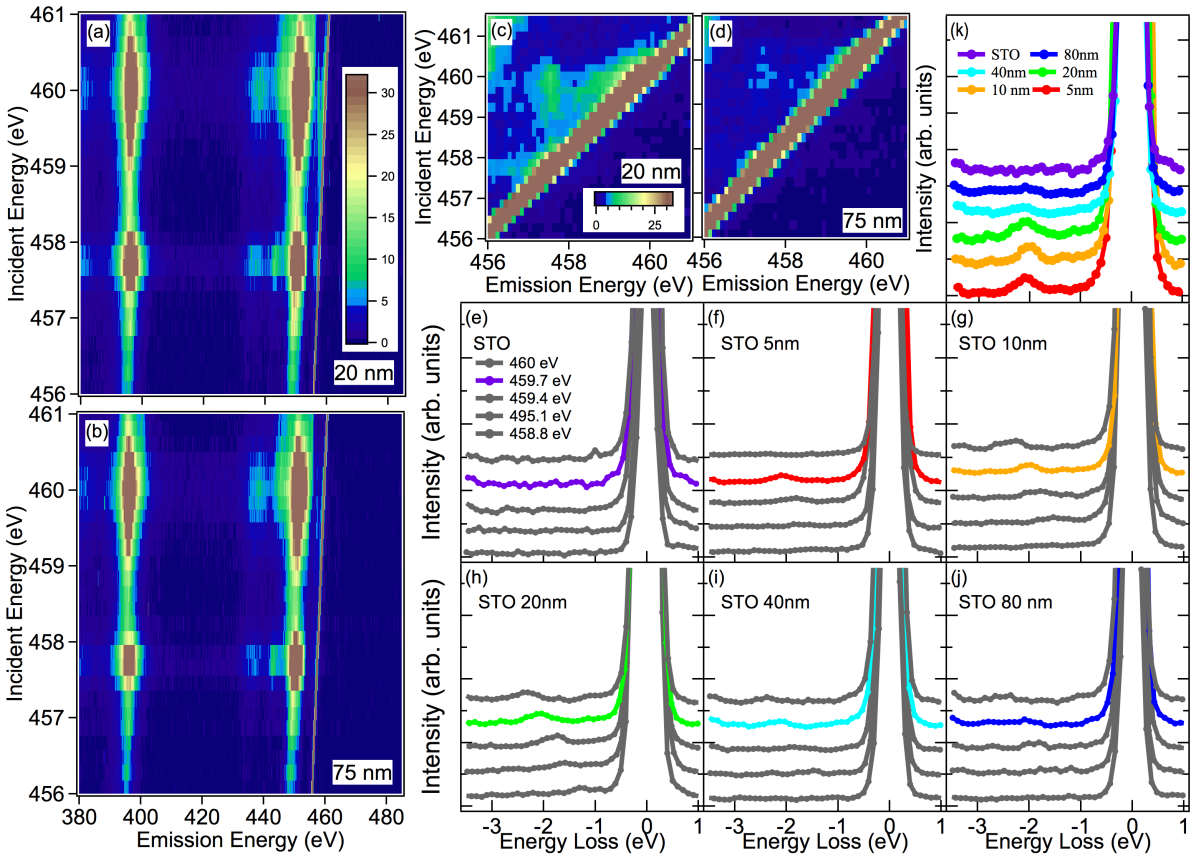

Figure 3. (a, b) 2D RIXS map of (a) 20 nm and (b) 75 nm STO-FS films with incident photon energy scanned across the Ti $L_{2,3}$-edge. (c, d) A zoomed-in view of the near elastic peak region highlighting the presence of a fluorescence-like feature in the 20 nm STO-FS. (e–k) Selected RIXS spectra with excitation photon energies around the Ti L_3–edge e_g threshold from (e) a bare STO substrate and STO-FS with (f) 5 nm, (g) 10 nm, (h) 20nm, (i) 40 nm, and (j) 80nm thickness. The

excitation photon energies are listed in panel (e). The colored spectra in panels (e) – (j) are compiled in panel (k) for comparison.

In these RIXS maps, we see a series of charge-transfer excitations that are 4 ~ 12 eV lower in emission energy than the elastic peak (zero energy loss).[36] Additional emissions that are ~ 60 eV away from the elastic peak come from the core-to-core transitions (Ti 3*s* -> 2*p* transitions, see Figure S3 in SI). Although both images show these generic features, the subtle difference can be revealed if zooming in the region around the elastic peak. Enhancing the contrast, we can identify an additional fluorescence-like feature at 457.6 eV emission energy in the RIXS map of a 20 nm STO-FS (Figure 3(c)). However, this feature is significantly suppressed in the 75 nm STO-FS (Figure 3(d)). In addition, we also see a spectral shoulder at < 1 eV energy loss in Figure 3(c) from inter-orbital (*dd*) excitation with *xz*/*yz* orbital character.[39] The fluorescence-like feature (denoted FL) and *dd* excitations both have a clear resonance behavior, confirming their origin from Ti 3*d* electrons and not the experimental artifacts. We focus on this FL feature and present selected RIXS spectra in Figure 3(e) - 3(j). The excitation photon energies for these spectra are chosen around the Ti L_3 e_g resonance as in other RIXS studies (see SI for more details).

Unlike RIXS measurements on LAO/STO where both localized (Raman-like) and delocalized (fluorescence-like) Ti 3*d* carries are visible in the 1 ~ 3 eV energy loss range,[36,37,39] our STO-FS RIXS spectra show the spectral feature coming mainly from the delocalized carriers. The intensity of FL around 2 eV energy loss is stronger in films with thickness less than 20 nm, and there is a significant suppression in 40 nm STO-FS (Figure 3(k)). Since the RIXS spectral intensity is proportional to the number of scatters,[40] the more intense FL implies a higher delocalized carrier

concentration. This FL feature is barely visible in 80 nm STO-FS (Figure 3(j)), and consistent with the literature,[36,40] we do not find it in bulk STO (Figure 3(e)).

Because of their similar energy loss scale and resonance onset, one may view this FL as the signature of some type of surface free carriers in our STO-FS as in the case of interfacial 2DEG in LAO/STO heterostructure. However, we argue that this FL feature is not merely caused by the surface carriers or other surface effects. Surface reconstruction from broken translation symmetry can change the Ti electronic structure, but the reconstruction is expected to be localized within a few unit cells around the surface region and depends on the surface termination.[41,42] Considering the normalization scheme employed in RIXS spectra that takes the number of photo-excited core holes into account (see SI), the comparable FL intensity in 5, 10, and 20 nm STO-FS films points to the bulk origin instead of the surface because the relative contribution from the surface will decrease with film thickness (Figure 3(k)).

There were angle-resolved photoemission spectroscopy (ARPES) reports of conducting carriers on the STO surface, but those samples had to be modified either by introducing additional oxygen vacancies during the growth or by UV irradiation.[26] The UV exposure enhances the surface electron density with time. In our study, we observed an opposite trend that long exposure to soft x-rays led to the suppression of FL spectral weight in 5 nm STO-FS. PLD growth at lower oxygen pressure ($<10^{-5}$ mbar) can make the STO film conductive while at higher oxygen pressure ($>10^{-5}$ mbar), STO becomes insulating.[43,44] Our films were grown at oxygen pressure higher than 10^{-1} mbar, hence they are expected to be insulating to begin with. We tried to measure the sheet resistance using the four-point method, but all STO-FS films exhibit insulating behavior with the sheet resistance higher than 100 MΩ per square.[45]

The spectral width of Ti-O hybridization feature in O *K*-edge XAS spectra was shown to change with oxygen vacancy concentration.[43] We have compared this width between bulk STO and STO-FS, see Figure 2(c). Although the intensity of t_{2g} and e_g hybridization features decreases with the reduced film thickness and the SiO_2 layer from Si wafer support gives a stronger background above 534 eV when the STO-FS film thickness is less than the x-ray probe depth (~ 50 nm), the half-width-half maximum (HWHM) at the lower energy side of this t_{2g} hybridization feature shows the negligible difference between these samples (see inset). The agreement rules out the scenario that our STO-FS films experienced severe oxygen loss in vacuum prior to the RIXS measurements to induce an enhanced FL feature.

Excluding scenarios based on extrinsic, growth, and surface effects to explain the enhanced FL signal in RIXS spectra, we look at the structure aspect. We notice that lowering the crystal symmetry from O_h to D_{4h} will change the Ti and O orbital characters near Fermi energy, as well as the degree of Ti-O hybridization and charge-transfer. As a result, the nominal 4+ valency assigned to Ti ion in bulk STO can be slightly different in our STO-FS. To elaborate on the evolution of Ti and O projected DOS (PDOS) with respect to the number of STO unit cells, we carried out density functional theory (DFT) calculations in the GGA framework (see SI).

Our calculation reveals several interesting findings. For unoccupied Ti PDOS, the states nearest to Fermi energy (0 eV) are from the *xy* orbital, and those from *xz*/*yz* orbitals are situated at 0.5 eV higher energy (leading edge, see Figure 4(a)). Such an energy difference associated with the tetragonal structure quickly diminishes when the number of STO layers is increased (3 vs 9 layers, see Figure 4(a) and Figure 4(b)) and is absent in bulk STO as expected. Enhancing the tetragonality leads to different downshifts of the centroid of unoccupied Ti t_{2g} and occupied O *p* orbitals, giving the impression of an increased band gap. However, the spectral weight at Fermi energy, which

comes from O p_x/p_y orbitals, behaves oppositely such that it is larger in the 3-layer configuration (Figure 4(c) and Figure 4(d)). The increased spectral weight suggests changes in the Ti-O hybridization. This prediction is verified by the valance band soft x-ray photoelectron spectroscopy (SXPES) on 5 nm and 10 nm STO-FS at room temperature. In Figure 4(f), we see the 5 nm spectrum exhibits more spectral weight close to Fermi energy than the 10 nm spectrum. Note that there is no quasiparticle-like sharp feature in these SXPES spectra, and this pseudogap-like spectral lineshape resembles the strange metal behavior in other correlated transition metal oxides. DFT calculation also predicts the room temperature tetragonality will increase with decreasing STO layers (Figure 4(e)), in agreement with the lattice constants in Figure 1(e).

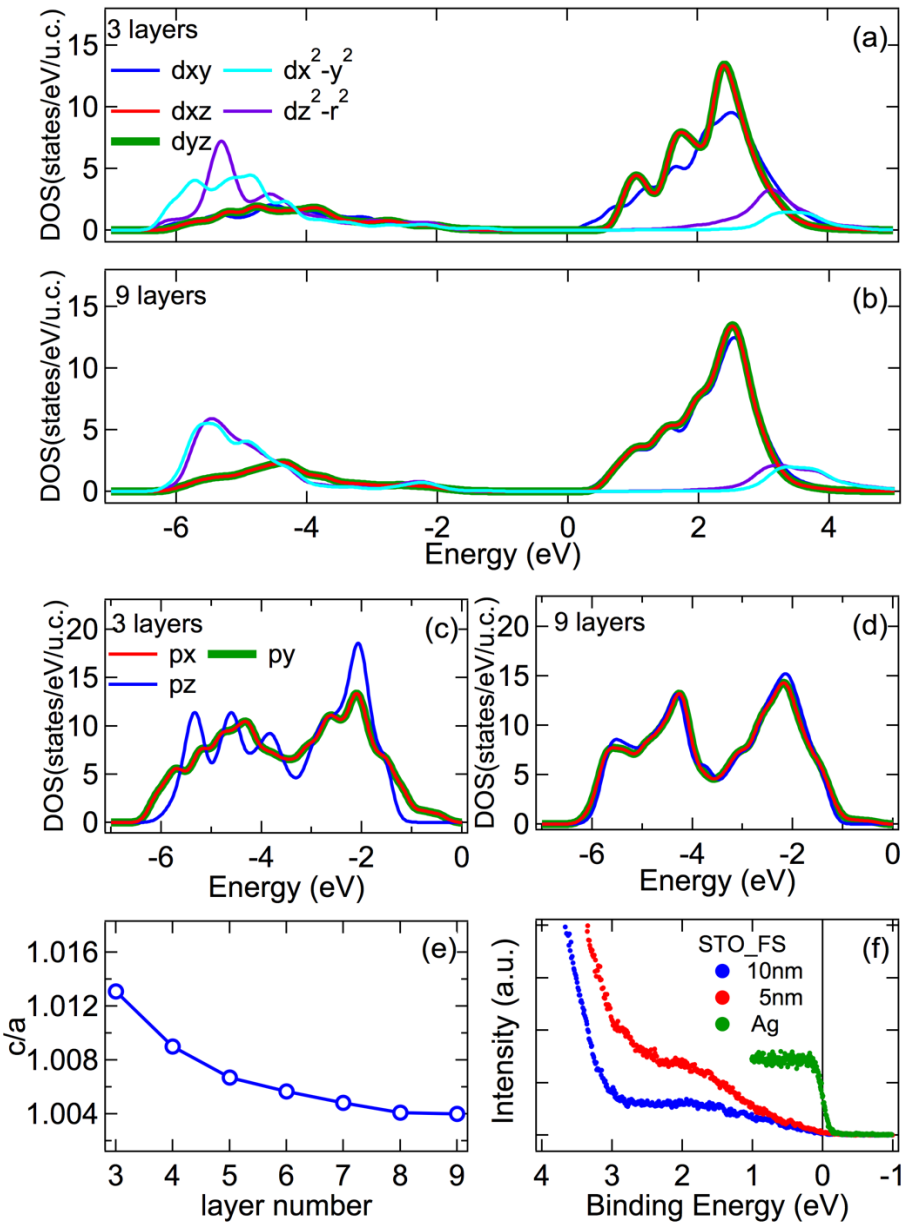

Figure 4. (a, b) Density of states (DOS) of Ti 3*d* orbitals in the (a) 3 and (b) 9 atomic-layer systems. (c, d) DOS of oxygen 2*p* orbitals in the (c) 3 and (d) 9 atomic-layer systems. (e) Lattice parameter (*c*/*a*) as a function of atomic layers showing the enhanced tetragonality with the reduced layer number. (f) Valence band SXPES spectra of 5 nm (red) and 10 nm (blue) STO-FS overlaid with the Fermi edge spectrum from Ag (green). The spectra were normalized using the featureless region 13 ~ 15 eV below the Fermi energy.

The SXPES, XAS, and RIXS results suggest that in the thin STO-FS, change in the Ti-O orbital (*pd*) hybridization causes the spectral weight transfer from unoccupied Ti t_{2g} manifold to form an in-gap state (IGS). This spectral weight evolution bears similarity to that of the Nb-doped STO reported by resonant PES.[46] In that PES study, the bulk incoherent IGS is proposed to come from the transferred spectral weight from the coherent state (CS), and the strong Ti-O *pd* hybridization induces the locally screened Ti^{3+} ($d^1\underline{L}$, $\underline{L}$ denotes the ligand hole). On the other hand, the coherent state responsible for electrical conduction has the dominant Ti t_{2g} character. We can borrow this picture to understand the spectral weight behavior in STO-FS. In this analogy, the CS becomes the unoccupied Ti t_{2g} manifold and the IGS is truly in the band gap (~ 3.2 eV). This analogy is reasonable because the intensity of FL feature in RIXS spectra anti-correlates with the spectral weight of two leading peaks in XAS spectra, and both show a clear change below 40 nm (see inset in Figure 2(a) and Figure 3(k)).

There are subtleties in this analogy that one should be aware of. One may qualitatively view this IGS in STO-FS as multiple charge states like in the transition metal doped semiconductors proposed by Haldane and Anderson,[47] but there is no extrinsic doping here except the modified *pd* hybridization by the inherent tetragonal instability. Although the observed FL feature has a similar energy scale and resonance behavior as the 2DEG in LAO/STO, one should refrain from assigning it to 2DEG because this notion implies a macroscopic metallic state that does not agree with the sheet resistance measurements. We also cannot unambiguously assert the length scale nor the magnitude of Ti^{3+} ($d^1\underline{L}$) state because of the lack of spatially resolved capability in spectroscopies. The observation of delocalized Ti 3*d* carriers may seem to contradict the insulating behavior in

STO-FS, but these probes operate at different frequency and momentum regimes, and they measure disparate correlation functions.

The room temperature tetragonality with Ti ion moving away from the central position in TiO_6 octahedron may favor the ferroelectricity, but our 5 nm STO-FS film fails to establish the stable, macroscopic ferroelectricity. TEM images show that such atomic displacement is not homogeneous within the field of view, and the heterogeneity is likely caused by the balance of Coulomb energies (see Figure S6 in SI). It has been shown that the strain-free STO film grown on a buffer $SrRuO_3$ (SRO) layer can display a relaxor ferroelectric behavior. As the STO film thickness approaches the length scale of polar nanoregions (~ 10 nm),[15,48] an applied electric field can stabilize the ferroelectricity at room temperature. It is suggested that PNRs help align the ferroelectric domains around this thickness scale. Our findings on STO-FS, absence of the influence from SRO buffer layer through the bridging O atoms, demonstrate the close connection between this intrinsic structure instability and the thickness scale where PNRs become prominent. Note that the observed Ti valency in STO-FS is inconsistent with the Sr deficiency scenario proposed for PNR. Our results also show that despite reducing the STO thickness may seem to be unfavorable for the ferroelectricity against the unscreened depolarization field,[49] the enhanced structural instability can deepen the potential well and facilitate the displacive transition,[50] allowing a more versatile control of ferroelectricity. One may envision that the enhancement of structural instability may depend on the crystalline orientation of freestanding films, for example, (001)-oriented versus (110)-oriented STO-FS. Based on the temperature-dependent structural transition in $BaTiO_3$, one can speculate the effect might be weaker in (110)-oriented STO-FS because the Ti ionic displacement will need to seek the balance between the competing tetragonal and orthorhombic (pseudo-cubic notation) instability and the displacement may not be completely

along the Ti-O bond direction. Verification of this conjecture may shed light on the understanding of nanoscopic structural response to crystalline engineering. We expect that by applying this freestanding treatment to other correlated oxides, one can better differentiate the intrinsic and substrate-induced structural and electronic responses to reduced dimensionality, which will be important for tailoring the functionalities of heterostructures.

ASSOCIATED CONTENT

Supporting Information.

XRD azimuthal scan, RIXS spectra normalization scheme, XLD measurement and configuration interaction cluster calculations, Ti $L_{2,3}$-edge XAS simulations, TEM images of a 10 nm freestanding STO film, DFT calculations, soft x-ray photoelectron spectroscopy spectra, and details of experimental methods (PDF).

AUTHOR INFORMATION

Corresponding Author

* Email: janchiyang@phys.ncku.edu.tw

* Email: shih.huang@psi.ch.

* Email: ychuang@lbl.gov

Present Addresses

|| National Synchrotron Radiation Research Center, Hsinchu 300, Taiwan

Author Contributions

S.W.H and Y.-D.C. conceived the idea. C.C.C., S.Z.H., Y.W.C., Y.C.L., and J.C.Y provided freestanding $SrTiO_3$ (STO-FS) and STO/LSMO/STO thin films, and performed transport, XRD, AFM, and STM characterization. Y.-D.C and Y.C.S performed the XAS and RIXS measurements. C.F.C. and C.Y.K. performed the XLD and SXPES measurements and the configuration interaction cluster calculations. R.H. processed TEM characterizations. Y.S. and C.G.D. performed the DFT calculations and HAADF-STEM measurements. S.W.H., J.M.L., C.F.C, and C.Y.K. analyzed the spectroscopic data. S.W.H., J.C.Y., and Y.-D.C. wrote up the manuscript through contributions of all authors. All authors have given approval to the final version of the manuscript. Δ These authors contribute equally in this work.

Funding Sources

Department of Energy, Contract No. DE-AC02-05CH11231

Ministry of Science and Technology (MOST) in Taiwan, MOST 110-2636-M-006-003 (Young Scholar Fellowship Program)

National Key Research and Development Program of China, 2017YFA0303403

National Natural Science Foundation of China, Grant No. 61974042

Higher Education Sprout Project, Ministry of Education of the Headquarters of University Advancement at National Cheng Kung University

Notes

The authors declare no competing financial interests

ACKNOWLEDGMENT

The Advanced Light Source is supported by the Director, Office of Science, Office of Basic Energy Sciences, of the U.S. Department of Energy under Contract No. DE-AC02-05CH11231. J.C.Y. acknowledges the financial support from Ministry of Science and Technology (MOST) in Taiwan under grant nos. MOST 110-2636-M-006-003 (Young Scholar Fellowship Program). R.H. is supported by the National Key Research and Development Program of China (2017YFA0303403) and the National Natural Science Foundation of China (Grant No. 61974042). C.C.C., Y.W.C., Y.C.L., and J.C.Y. are supported in part by Higher Education Sprout Project, Ministry of Education of the Headquarters of University Advancement at National Cheng Kung University (NCKU). The experiments at the Taiwan Photon Source in Taiwan were facilitated by the Max Planck - POSTECH - Hsinchu Center for Complex Phase Materials.

REFERENCES

(1) Muller, K. A.; Burkard, H. $SrTiO_3$: An intrinsic quantum paraelectric below 4 K. *Phys. Rev. B* **1979**, *19*, 3593-3602.

(2) Cochran, W. Crystal stability and the theory of ferroelectricity. *Advances in Physics* **1960**, *9*, 387-423.

(3) Pai, Y. Y.; Tylan-Tyler, A.; Irvin, P.; Levy, J. Physics of $SrTiO_3$-based heterostructures and nanostructures: a review. *Rep. Prog. Phys.* **2018**, *81*, 036503.

(4) Dawber, M.; Rabe, K. M.; Scott, J. F. Physics of thin-film ferroelectric oxides. *Rev. Mod. Phys.* **2005**, *77*, 1083-1130.

(5) Hwang, H. Y.; Iwasa, Y.; Kawasaki, M.; Keimer, B.; Nagaosa, N.; Tokura, Y. Emergent phenomena at oxide interfaces. *Nature Materials* **2012**, *11*, 103-113.

(6) Zubko, P.; Gariglio, S.; Gabay, M.; Ghosez, P.; Triscone, J. -M. Interface physics in complex oxide heterostructures. *Annu. Rev. Condens. Matter Phys.* **2011**, *2*, 141-165.

(7) Ohtomo, A.; Hwang, H. Y. A high-mobility electron gas at the LaAlO /SrTiO heterointerface. *Nature* **2004**, *427*, 423-426.

(8) Thiel, S.; Hammerl, G.; Schmehl, A.; Schneider, C. W.; Mannhart, J. Tunable Quasi–Two-Dimensional Electron Gases in Oxide Heterostructures. *Science* **2006**, *313*, 1942-1945.

(9) Brinkman, A.; Huijben, M.; van Zalk, M.; Huijben, J.; Zeitler, U.; Maan, J. C.; van der Wiel, W. G.; Rijnders, G.; Blank, D. H. A.; Hilgenkamp, H. Magnetic effects at the interface between non-magnetic oxides. *Nature Materials* **2007**, *6*, 493-496.

(10) Reyren, N.; Thiel, S.; Caviglia, A. D.; Fitting Kourkoutis, L.; Hammerl, G.; Richter, C.; Schneider, C. W.; Kopp, T.; Rüetschi, A. -S.; Jaccard, D.; Gabay, M.; Muller, D. A.; Triscone, J.-M.; Mannhart, J. Superconducting interfaces between insulating oxides. *Science* **2007**, *317*, 1196-1199.

(11) Caviglia, A. D.; Gariglio, S.; Reyren, N.; Jaccard, D.; Schneider, T.; Gabay, M.; Thiel, S.; Hammerl, G.; Mannhart, J.; Triscone, J.-M. Electric field control of the $LaAlO_3/SrTiO_3$ interface ground state. *Nature* **2008**, *456*, 624-627.

(12) Ohtomo, A.; Muller, D. A.; Grazul, J. L.; Hwang, H. Y. Artificial charge-modulation in atomic-scale perovskite titanate superlattices. *Nature* **2002**, *419*, 378-380.

(13) Stemmer, S.; Allen, S. J. Two-dimensional electron gases at complex oxide interfaces. *Annu. Rev. Mater. Res.* **2014**, *44*, 151-171.

(14) Huang, D.; Hoffman, J. E. Monolayer FeSe on $SrTiO_3$. *Annu. Rev. Condens. Matter Phys*. **2017**, *8*, 311-336.

(15) Lee, D. -H. Routes to high-temperature superconductivity: a lesson from FeSe/$SrTiO_3$. *Annu. Rev. Condens. Matter Phys.* **2018**, *9*, 261-282.

(16) Okamoto, S.; Millis, A. J. Electronic reconstruction at an interface between a Mott insulator and a band insulator. *Nature* **2004**, *428*, 630-633.

(17) Nakagawa, N.; Hwang, H. Y.; Muller, D. A. Why some interfaces cannot be sharp. *Nature Materials* **2006**, *5*, 204-209.

(18) Xu, R.; Huang, J.; Barnard, E. S.; Hong, S. S.; Singh, P.; Wong, E. K.; Jansen, T.; Harbola, V.; Xiao, J.; Wang, B. Y.; Crossley, S.; Lu, D.; Liu, S.; Hwang, H. Y. Strain-induced room-temperature ferroelectricity in $SrTiO_3$ membranes. *Nature Comm*. **2020**, *11*, 3141.

(19) Nova, T. F.; Disa, A. S.; Fechner, M.; Cavalleri, A. Metastable ferroelectricity in optically strained $SrTiO_3$. *Science* **2019**, *364*, 1075-1079.

(20) Haeni, J. H.; Irvin, P.; Chang, W.; Uecker, R.; Reiche, P.; Li, Y. L.; Choudhury, S.; Tian, W.; Hawley, M. E.; Craigo, B.; Tagantsev, A. K.; Pan, X. Q.; Streiffer, S. K.; Chen, L. Q.; Kirchoefer, S. W.; Levy, J.; Schlom, D. G. Room-temperature ferroelectricity in strained $SrTiO_3$. *Nature* **2004**, *430*, 758-761.

(21) Lee, D.; Lu, H.; Gu, Y.; Choi, S. -Y.; Li, S. -D.; Ryu, S.; Paudel, T. R.; Song, K.; Mikheev, E.; Lee, S.; Stemmer, S.; Tenne, D. A.; Oh, S. H.; Tsymbal, E. Y.; Wu, X.; Chen, L. -Q.; Gruverman, A.; Eom, C. B. Emergence of room-temperature ferroelectricity at reduced dimensions. *Science* **2015**, *349*, 1314-1317.

(22) Itoh, M.; Wang, R.; Inaguma, Y.; Yamaguchi, T.; Shan, Y. -J.; Nakamura, T. Ferroelectricity induced by oxygen isotope exchange in strontium titanate perovskite. *Phys. Rev. Lett.* **1999**, *82*, 3540-3543.

(23) Hemberger, J.; Lunkenheimer, P.; Viana, R.; Bohmer, R.; Loidl, A. Electric-field-dependent dielectric constant and nonlinear susceptibility in $SrTiO_3$. *Phys. Rev. B* **1995**, *52*, 13159-13162.

(24) Gastiasoro, M. N.; Ruhman, J.; Fernandes, R. M. Superconductivity in dilute $SrTiO_3$: A review. *Annals of Physics* **2020**, *417*, 168107.

(25) Ahadi, K.; Galletti, L.; Li, Y.; Salmani-Rezaie, S.; Wu, W.; Stemmer, S. Enhancing superconductivity in $SrTiO_3$ films with strain. *Science Advances* **2019**, *5*, eaaw0120.

(26) Santander-Syro, A. F.; Copie, O.; Kondo, T.; Fortuna, F.; Pailhes, S.; Weht, R.; Qiu, X. G.; Bertran, F.; Nicolaou, A.; Taleb-Ibrahimi, A.; Le Fevre, P.; Herranz, G.; Bibes, M.; Reyren, N.; Apertet, Y.; Lecoeur, P.; Barthelemy, A.; Rozenberg, M. J. Two-dimensional electron gas with universal subbands at the surface of $SrTiO_3$. *Nature* **2011**, *469*, 189-193.

(27) Meevasana, W.; King, P. D. C.; He, R. H.; Mo, S. -K.; Hashimoto, M.; Tamai, A.; Songsiriritthigul, P.; Baumberger, F.; Shen, Z. -X. Creation and control of a two-dimensional electron liquid at the bare SrTiO3 surface. *Nature Materials* **2011**, *10*, 114-118.

(28) Basletic, M.; Maurice, J. -L.; Carretero, C.; Herranz, G.; Copie, O.; Bibes, M.; Jacquet, E.; Bouzehouane, K.; Fusil, S.; Barthelemy, A. Mapping the spatial distribution of charge carriers in $LaAlO_3/SrTiO_3$ heterostructures. *Nature Materials* **2008**, **7**, 621-625.

(29) Kroll, T.; Solomon, E. I.; de Groot, F. M. F. Final-state projection method in charge-transfer multiplet calculations: an analysis of Ti L-edge absorption spectra. *J. Phys. Chem. B* **2015**, *119*, 13852-13858.

(30) de Groot, F. M. F.; Fuggle, J. C.; Thole, B. T.; Sawatzky, G. A. $L_{2,3}$ x-ray absorption edges of d^0 compounds: K^+, Ca^{2+}, Sc^{3+}, and Ti^{4+} in O_h (octahedral) symmetry. *Phys. Rev. B* **1990**, *41*, 928-937.

(31) Stohr, J.; Siegmann, H. C. *Magnetism*, Springer, 2006.

(32) Pertsev, N. A.; Zembilgotov, A. G.; Tagantsev, A. K. Effect of mechanical boundary conditions on phase diagrams of epitaxial ferroelectric thin films. *Phys. Rev. Lett*. **1998**, *80*, 1988-1991.

(33) Lin, C. -H.; Huang, C. -M.; Guo, G. Y. Systematic ab initio study of the phase diagram of epitaxially strained $SrTiO_3$. *J. App. Phys*. **2006**, *100*, 084104.

(34) Altmeyer, M.; Jeschke, H. O.; Hijano-Cubelos, O.; Martins, C.; Lechermann, F.; Koepernik, K.; Santander-Syro, A. F.; Rozenberg, M. J.; Valentí, R.; Gabay, M. Magnetism, spin texture, and in-gap states: atomic specialization at the surface of oxygen-deficient $SrTiO_3$. *Phys. Rev. Lett.* **2016**, *116*, 157203.

(35) Plumb, N. C.; Salluzzo, M.; Razzoli, E.; Mansson, M.; Falub, M.; Krempasky, J.; Matt, C. E.; Chang, J.; Schulte, M.; Braun, J.; Ebert, H.; Minar, J.; Delley, B.; Zhou, K. -J.; Schmitt, T.; Shi, M.; Mesot, J.; Patthey, L.; Radovi, M. Mixed dimensionality of confined conducting electrons in the surface region of $SrTiO_3$. *Phys. Rev. Lett*. **2014**, *113*, 086801.

(36) Pfaff, F.; Fujiwara, H.; Berner, G.; Yamasaki, A.; Niwa, H.; Kiuchi, H.; Gloskovskii, A.; Drube, W.; Gabel, J.; Kirilmaz, O.; Sekiyama, A.; Miyawaki, J.; Harada, Y.; Suga, S.; Sing, M.; Claessen, R. Raman and fluorescence contributions to the resonant inelastic soft x-ray scattering on $LaAlO_3/SrTiO_3$ heterostructures. *Phys. Rev. B* **2018**, *97*, 035110.

(37) Zhou, K. -J.; Radovic, M.; Schlappa, J.; Strocov, V.; Frison, R.; Mesot, J.; Patthey, L.; Schmitt, T. Localized and delocalized Ti 3dcarriers in $LaAlO_3/SrTiO_3$ superlattices revealed by resonant inelastic x-ray scattering. *Phys. Rev. B* **2011**, *83*, 201402(R).

(38) Geondzhian, A.; Sambri, A.; De Luca, G. M.; Di Capua, R.; Di Gennaro, E.; Betto, D.; Rossi, M.; Peng, Y. Y.; Fumagalli, R.; Brookes, N. B.; Braicovich, L.; Gilmore, K.; Ghiringhelli, G.; Salluzzo, M. Large polarons as key quasiparticles in $SrTiO_3$ and $SrTiO_3$-based heterostructures. *Phys. Rev. Lett*. **2020**, *125*, 126401.

(39) Lin, S. -C.; Kuo, C. -T.; Shao, Y. -C.; Chuang, Y. -D.; Geessinck, J.; Huijben, M.; Rueff, J. -P.; Graff, I. L.; Conti, G.; Peng, Y. Y.; Bostwick, A.; Rotenberg, E.; Gullikson, E.; Nemsak, S.; Vailionis, A.; Gauquelin, N.; Verbeeck, J.; Ghiringhelli, G.; Schneider, C. M.; Fadley, C. S. Two-dimensional electron systems in perovskite oxide heterostructures: role of the polarity-induced substitutional defects. *Phys. Rev. Mater*. **2020**, *4*, 115002.

(40) Berner, G.; Glawion, S.; Walde, J.; Pfaff, F.; Hollmark, H.; Duda, L.-C.; Paetel, S.; Richter, C.; Mannhart, J.; Sing, M.; Claessen, R. $LaAlO_3/SrTiO_3$ oxide heterostructures studied by resonant inelastic x-ray scattering *Phys. Rev. B* **2010**, *82*, 241405(R).

(41) Ravikumar, V.; Wolf, D.; Dravid, V. P. Ferroelectric-monolayer reconstruction of the $SrTiO_3$ (100) surface. *Phys. Rev. Lett.* **1995**, *74*, 960-963.

(42) Herger, R.; Willmott, P. R.; Bunk, O.; Schleputz, C. M.; Patterson, B. D.; Delley, B. Surface of strontium titanate. *Phys. Rev. Lett*. **2007**, *98*, 076102.

(43) Siemons, W.; Koster, G.; Yamamoto, H.; Harrison, W. A.; Lucovsky, G.; Geballe, T. H.; Blank, D. H. A.; Beasley, M. R. Origin of charge density at $LaAlO_3$ on $SrTiO_3$ heterointerfaces: possibility of intrinsic doping. *Phys. Rev. Lett*. **2007**, *98*, 196802.

(44) Herranz, G.; Basletic, M.; Bibes, M.; Carretero, C.; Tafra, E.; Jacquet, E.; Bouzehouane, K.; Deranlot, C.; Hamzic, A.; Broto, J. -M.; Barthelemy, A.; Fert, A. High mobility in $LaAlO_3/SrTiO_3$ heterostructures: origin, dimensionality, and perspectives. *Phys. Rev. Lett.* **2007**, *98*, 216803.

(45) Lin, X.; Rischau, C. W.; Buchauer, L.; Jaoui, A.; Fauqué, B.; Behnia, K. Metallicity without quasi-particles in room-temperature strontium titanate. *npj Quantum Mater*. **2017**, *2*, 41.

(46) Ishida, Y.; Eguchi, R.; Matsunami, M.; Horiba, K.; Taguchi, M.; Chainani, A.; Senba, Y.; Ohashi, H.; Ohta, H.; Shin, S. Coherent and incoherent excitations of electron-doped $SrTiO_3$. *Phys. Rev. Lett*. **2008**, *100*, 056401.

(47) Haldane, F. D. M.; Anderson, P. W. Simple model of multiple charge states of transition-metal impurities in semiconductors. *Phys. Rev. B* **1976**, *13*, 2553.

(48) Jang, H. W.; Kumar, A.; Denev, S.; Biegalski, M. D.; Maksymovych, P.; Bark, C. W.; Nelson, C. T.; Folkman, C. M.; Baek, S. H.; Balke, N.; Brooks, C. M.; Tenne, D. A.; Schlom, D. G.; Chen, L. Q.; Pan, X. Q.; Kalinin, S. V.; Gopalan, V.; Eom, C. B. Ferroelectricity in strain-free SrTiO3 thin films. *Phys. Rev. Lett*. **2010**, *104*, 197601.

(49) Lichtensteiger, C.; Triscone, J. M.; Junquera, J.; Ghosez, P. Ferroelectricity and tetragonality in ultrathin $PbTiO_3$ films. *Phys. Rev. Lett*. **2005**, *94*, 047603.

(50) Dove, M. T. Theory of displacive phase transitions in minerals *American Mineralogist* **1997**, *82*, 213-244.

TOC Figure

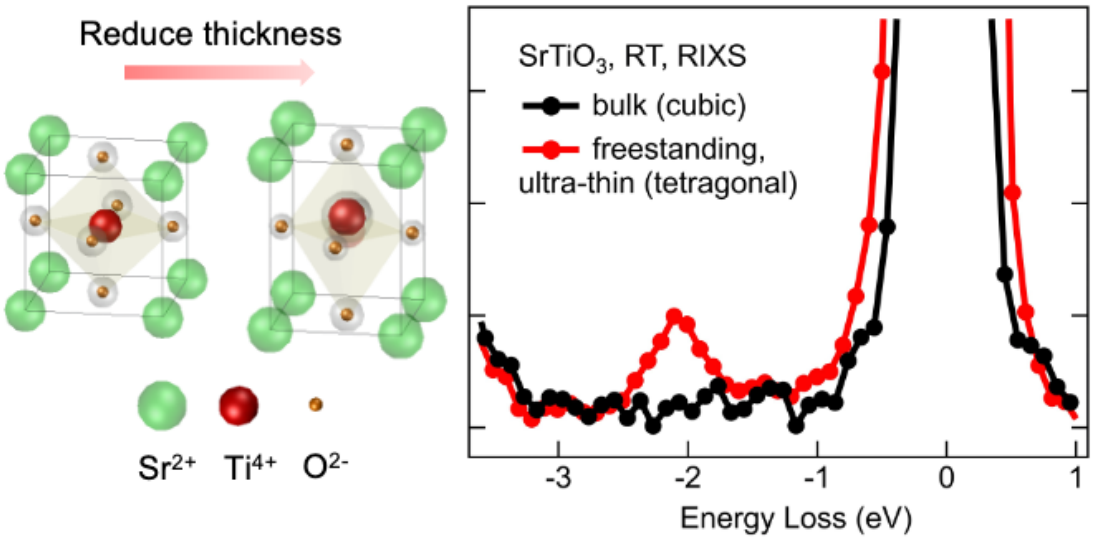
Reduce thickness
Sr2+ Ti4+ O2-
SrTiO3, RT, RIXS
bulk (cubic)
freestanding,
ultra-thin (tetragonal)
-3
-2
-1
0
1
Energy Loss (eV)